Characterization Of Carbon Nanotubes Coated Monolith Synthesized Via Chemical Vapor Deposition

Omar Qistina[1,4], Ali Salmiaton[1,2*], Thomas S.Y. Choong[1,2], Shamsul Izhar[1,2], and Yun Hin Taufiq-Yap[3]

[1] *Department of Chemical & Environmental Engineering, Faculty of Engineering, Universiti Putra Malaysia, 43400 Serdang, Selangor, Malaysia*
[2] *Sustainable Process Engineering Research Centre, Universiti Putra Malaysia, 43400 Serdang, Selangor, Malaysia*
[3] *Catalysis Science and Technology Research Centre, Faculty of Science, Universiti Putra Malaysia, 43400 Serdang, Selangor, Malaysia*
[4] *Centre of Foundation Studies, Universiti Teknologi MARA, Cawangan Selangor, Kampus Dengkil, 43800 Dengkil, Selangor, Malaysia*
[*] *Corresponding author. E-mail: mie@upm.edu.my*

Received: Oct. 16, 2023; Accepted: Jan. 09, 2024

Carbon nanotubes (CNTs) have been used as catalyst support in various catalytic activity. The existing CNTs in powder form can create high back pressure and inconvenient operational. Therefore, CNTs coated onto monolith structure provides a promising support for catalyst. In this study, the CNT monolith was synthesized using a chemical vapor deposition (CVD) method with deposition catalyst techniques determined by immersion and impregnation method. The synthesized CNTs monolith were characterized for surface morphology analysis, atomic composition, thermal stability, textural properties, functional group determination and crystallinity. The findings show that the CNTs formed are considered mesoporous nanotubes that attained a diameter size distribution scattered between 30 nm and 35 nm. The carbon yield was successfully achieved at more than 95% by the double immersion in the preparation technique. The CNTs monolith showed a very weak peak due to poor infrared transmittance, while the surface analysis of the CNTs monolith exhibited the type IV isotherm with H3 hysteresis in the presents of mesoporous structures with a relative pressure range of P/Po >0.4. The peak at 2 = 26.46° of the XRD pattern demonstrated a decrease after the synthesizing of CNTs growth onto monolith structure due to the production of carbon. The thermal analysis of the CNTs monolith showed a weight loss of moisture and organic residue of 0.13% and 3%, respectively. The results displayed an optional synthesis method and characterization information of CNTs structured monolith as value added for future production and application.

Keywords: carbon nanotubes; monolith; immersion; nickel; chemical vapor deposition

http://dx.doi.org/10.6180/jase.202501_28(1).0002

1. Introduction

Recently, the CNTs have attracted much interest in various fields including electronics [1, 2], energy storage [3, 4], material science [5], biomedical application [6, 7], coatings [8], and textiles [9]. The outstanding features of CNTs due to their high surface area, tubular structure, high mechanical strength, and unique electronic properties make them advantageous in a wide range of potential applications [10, 11]. Thus, CNTs possess high absorption abilities, adjustable mesoporosity, specific metal-support interactions, effective catalytic performance, and excellent selectivity

[12]. CNTs are generally synthesized using arc discharge [13, 14], laser ablation [15, 16], and chemical vapor deposition (CVD) [17, 18]. However, CVD is the most applicable technique to be commercialized as its ability to operate at low temperatures rather than laser ablation and the arc discharge method, which are normally conducted at high pressure [19]. CVD is cost effective for large-scale CNT synthesis process. However, the cost can vary depending on the specific process and material used as the carbon precursor is a significant factor for the final product price. Isaacs et al. [20] have analyzed the manufacturing cost of single-walled CNTs production in the increment order for HiPco, CVD and arc. The cost of each SWNT manufacturing process was dominated by the direct labor costs associated with the synthesis and filtration steps.

NTs are grown into arrays (forests), yarns, sheets, and sponges by different synthesis methods. The CNTs can be categorized as single-walled and multiwalled with a variety of morphology. In general, three morphologies of CNTs have been observed in directly grown nanotube array including horizontally, vertically, and entangled aligned. The horizontally alignment CNTs grown on a flat substrate and parallel to substrate with large intertube distance [21]. While, the vertically aligned CNTs have oriented perpendicular to the substrate surface with more uniform diameter and easily functionalized for a variety application [22, 23]. The entangled CNTs network also represents the Y-junctions, knotted and bridging structure which creates unique properties and potential application. The entangled or vertically aligned CNTs are practically impossible to obtain perfect structures and longer lengths up to centimeters [21].

Carbon source and catalyst play an important role in synthesizing CNTs. Each carbon source gives a different process in a synthesis reactor due to variations in the thermal transformation mechanism of organic substances from various classes [24]. Numerous hydrocarbons, such as methane [25], ethane [26], propane [27], polypropylene [28], ethylene [29, 30], acetone [24], and furfuryl alcohol [31, 32], are used as carbon sources. The noble metals (such as gold (Au)) and poor metals (such as Indium (In) and lead (Pb)) have been effective in CNTs growth [33]. However, metal catalyst nickel (Ni), iron (Fe), and cobalt (Co) are very active towards catalytic activity compared to noble metal series.

Ni-containing compounds commonly play a crucial role in the synthesize of CNTs via CVD method due to high solubility of carbon at high temperature and high carbon diffusion rate. Lim et al. [34] found the Ni have demonstrated the improvement in CNTs growth rates and crystallinity. Hence, the presence of catalyst can improve the yield and quality of CNTs [35]. Moreover, the Ni catalyst prominently displays great anti-sintering properties, higher activity, and low cost [10, 36]. Commonly, the metal catalyst will combine with carbon to form CNTs and serves as a seed to make carbon that has been deposited on the catalyst more stable and accumulate in sufficient quantities for crystalline growth. The production of CNT could increase in the presence of catalysts that provide good catalytic activity for the decomposition of hydrocarbons [37].

The CNTs growth have been discovered on sheets, fibers, films, and pellets. Some studies used metallic substrates, zeolite supports and ceramic as templates. The monolith structure can provide greater benefits such as improved mass transfer, reusability, high catalyst dispersion, high adsorption capacity and stability compared to powder and pellets [38]. Minett et al. [12] also investigated the growth of long CNT arrays onto monolith support. The idea of combination of monolith and CNTs offers higher specific area and low pressure making them suitable support for the industrial catalysis.

Additionally, the reaction conditions like precursor gas flowrate, process time and reaction temperature are also important factors in the CNTs growth development. The common techniques of catalyst deposition are wet impregnation, injection, floating catalyst, and co-precipitation. However, not all deposition techniques are appropriate for a monolith structure to retain its strength after the synthesizing process. Therefore, the novel approach of the study to growth of CNTs onto monolith using direct liquid injection CVD with a suitable deposition method for monolith structure and in-depth characterizing the synthesized CNTs.

2. Experimental setup

2.1. Chemical and materials

Direct fluid injection process of CVD was used to synthesize CNTs monolith catalyst. The 100 (L) mm x 25 (D) mm cordierite monolith ($2MgO{\cdot}Al_2O_3 \cdot 5SiO_2$) with 400 cells per square inch of cell density was purchased from Beihai Haihuang Chemical Packing Co. Ltd., China, and was cut into 10 mm (L) x 10 mm (D) in the preparation of CNTs monolith. All analytical-grade chemicals, such as nickel nitrate hexahydrates ($\geq$ 97%), furfuryl alcohol ($\geq$ 98%), citric acid ($\geq$ 99%), and ethanol ($\geq$ 99%), were purchased from Systerm Chemicals and used as received without further purification. The catalyst layer onto monolith was deposited with mixtures of nickel nitrate salts and citric acid in the distilled water. The carbon source was liquid furfuryl alcohol. The synthesis reaction was carried out in

a Carbolite horizontal quartz reactor using carrier gases ($<$ 98% purity of industrial nitrogen (N_2) and 99.9% purity of purified hydrogen (H_2)) provided by Smart Biogas Enterprise.

2.2. Synthesis of CNTs

The cordierite monolith was immersed in a 50:50 solution of ethanol and distilled water in a sonicator at 80 °C for an hour before being dried for an entire night at 120 °C. A mixed solution of Ni nitrate salts and citric acid at a ratio of 1:1 as 0.02 mol of Ni metal in solution was prepared. The first preparation method, the clean monolith was immersed into the mixed solution for an hour to ensure the dispersion of metal onto monolith pores. After that, the remaining solution was driven off using an air compressor to obtain a homogeneous catalytic layer and was dried overnight at 120 °C. The monolith of the immersion process was performed by two cycles to deposit more Ni on the monolithic surface. Both the immersion and the calcination processes were repeated to finish the second cycle. While as the second preparation method, the monolith was impregnated in mixed solution for overnight in an oven for 120 °C. In converting the $Ni(NO_3)_2$ deposited onto the monolith to NiO, both prepared monoliths were calcined at 450 °C for three hours. Then, the NiO monolith was subjected to the growth of CNTs in a tubular tube of chemical vapor deposition (CVD). The CVD was fixed properly, and the tube was purged with nitrogen gas before the temperature was set at 700 °C. Once the temperature had reached the setting temperature, the carrier gases (N_2andH_2) were started to flow at 100 sccm each, and the furfuryl alcohol (5 mL) was injected using a 20-inch-long needle at a fixed flow rate (0.034 ml/min) into the tube. After the injection was completed, the N_2 gas flow rate was increased to 500 sccm while H_2 gas flow rate remained at 100 sccm. The synthesis process of CNTs was conducted for 30 minutes and cooled down to room temperature after the reaction was completed. The synthesis method was conducted at optimum conditions obtained from the Taguchi method, as reported in the earlier work [39].

2.3. Characterization of CNTs

Field Emission Scanning Electron Microscopy (FESEM) (Thermo Scientific model Nova Nano 230) attached to the Energy-Dispersive X-ray (EDX) (Oxford Instruments) was used to observe the morphology and elemental atomic composition of CNTs catalyst. The analysis of the morphology features samples was employed using transmission electron microscopy (TEM, Hitachi H-7100). Prior to the TEM analysis, the samples were prepared by ultrasonic dispersion in absolute ethanol before placing it on the copper grid for 30 minutes and let it dry in air. The textural properties of the catalyst such as specific surface area, pore-volume, and pore size of catalysts were determined using Micromeritics 3Flex Version 1.02. The thermal stability of CNTs catalysts was examined by Thermogravimetric Analyser (TGA; TA instrument Q50) at temperatures up to 900°C in the air by a 10°C/min heating rate. The X ray diffraction (XRD) (Philips Expert PW3040) with the operating condition at 40kV and 40 mA with CuK$\alpha(\lambda = 1.5406)$ radiation source within 2θ range from 20 to 80° with a 0.033°/min step size was utilized to analyze the crystalline phases of the supports and catalysts.

3. Result discussions

In synthesizing of CNTs onto monolithic surface, the deposition technique of the metal catalyst onto the support structure is crucial needs to be considered as to maintain the strength and stability of the structure. The best technique is required to evenly disperse the metal catalyst onto the monolithic surface which resulting in a high CNT yield. Hence, the CNT monolith was investigated by two different methods: immersion and impregnation. The results showed that the CNT monolith structure prepared by the impregnation method was brittle as compared to the one prepared by the immersion method, as shown in Fig. 1. These results were consistent with the findings of Nijhuis et al. [40] that the doping of the metal catalyst via the immersion technique was the best for cordierite monolith as the structure strength was retained even after the synthesis of CNTs via CVD at 700 °C. The repetition in immersion can improve the amount carbon yield on the surface because more metal was deposited on the monolith's surface [40]. The resFig. 2.

3.1. Morphological analysis of CNTs monolith

The surface morphology and microstructure of the CNTs monolith were illustrated by FESEM and HRTEM analyses. The morphology analysis of the bare cordierite monolith and the CNT growth onto monolith at optimum condition shown in Fig. 3 was examined by the FESEM. CNTs growth could be individually and continuously depending on the preparation and synthesis method. The immersion method is considered as a pre-deposited catalyst layer on the support. As the CVD reached the setting temperature, the catalyst started to melt and shrank into nanoscale particles. Afterwards, the furfuryl alcohol as a carbon source was injected into the CVD tube, settled on the surface of the catalyst for the nanoparticles, and began to break down into carbon species. The droplet of carbon that transformed

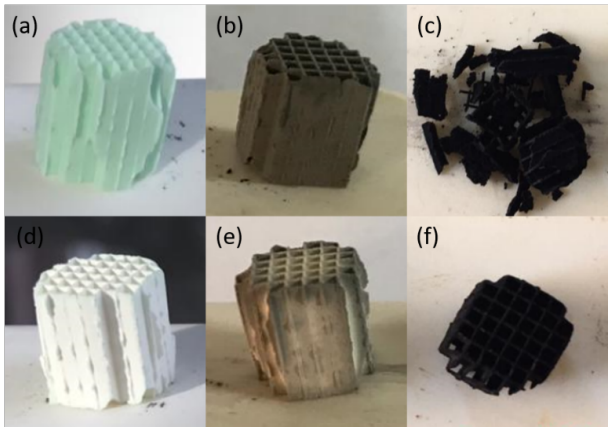

Fig. 1. The structure of CNTs monolith prepared by impregnation method ((a) after impregnation process; (b) after calcination at 450 °C; (c) CNTs produced) and immersion method ((d) after immersion process; (e) after calcination at 450 °C; (f) CNTs produced).

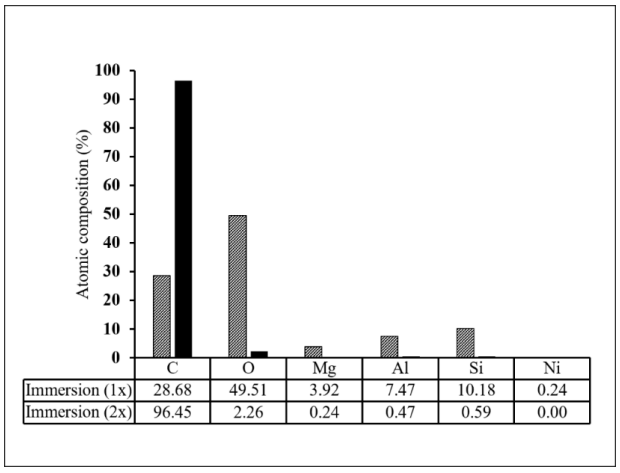

	C	O	Mg	Al	Si	Ni
Immersion (1x)	28.68	49.51	3.92	7.47	10.18	0.24
Immersion (2x)	96.45	2.26	0.24	0.47	0.59	0.00

Fig. 2. The EDX analysis for the doping method via immersion method.

into vapor was placed at a preferred location, reached a saturation threshold, and lifted the carbon to start the crystal's development. The catalyst acted like a sock for carbon atom which traveled through the CVD and deposited on the support surfaces directly [41]. Thus, the CNTs nucleated on them. The length of the CNTs most likely relied on the catalyst's and carbon source's structures. The polyaromatic hydrocarbon generated longer CNTs and was easily graphitized [42].

The synthesized-CNTs in this study are unpurified ones and inevitably contain carbonaceous impurities and metal catalyst particles. The impurities commonly increase with the decrease of CNT diameter [43]. The CNTs on the monolith revealed the diameter size distribution at 60 sites, with the largest size distribution of CNTs falling within the range of 30 to 35 nm, which is equivalent to mesoporous nanotubes. The diameter distribution of tubes is more uniform, probably less amorphous carbon and fewer tube defects. The production of CNTs with a narrow distribution of diameter was contributed by more uniform and small Ni nanoparticles dispersed onto the surface, which also aligned with the finding by He et al. [44].

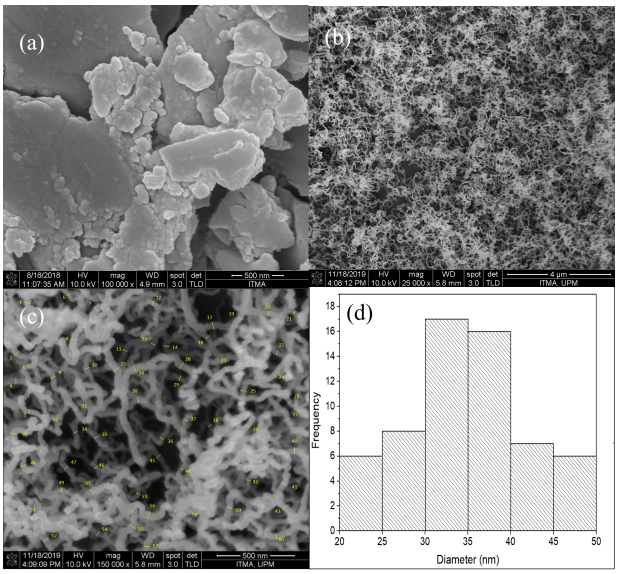

Fig. 3. Micrograph image of (a) bare cordierite monolith, (b) CNT monolith at 25000 magnifications, (c) CNT monolith at 150000 magnifications, and (d) size distribution of CNTs in nm.

The HRTEM images have revealed the microstructure of CNTs with several sizes. From the images, the CNT arrays are entangled aligned composed of randomly oriented nanotubes that are linked together. In this work, the CNTs can be seen clearly knotted as shown in Figs. 3 and 4. The analysis indicated the presence of Ni-filled tubes, which showed that CNTs grow through a tip growth mechanism on monolithic surfaces, as shown in Fig. 3. The mechanism demonstrated that the metal support interaction was weak and contributed to tip growth mode [45, 46].

3.2. Chemical analysis of CNTs monolith

The FTIR spectra showed the frequencies of absorption radiation, which are differentiated for each molecule, bonded strength, atom number, condition of material as a state, interference contamination, concentration, temperature multiples, and bending and stretching vibration modes. Fig. 5 shows the FTIR analysis of bare cordierite monolith, furfuryl alcohol as carbon source, and CNTs monolith measured within a range from 4000 to 700 cm^{-1}. Spectrums

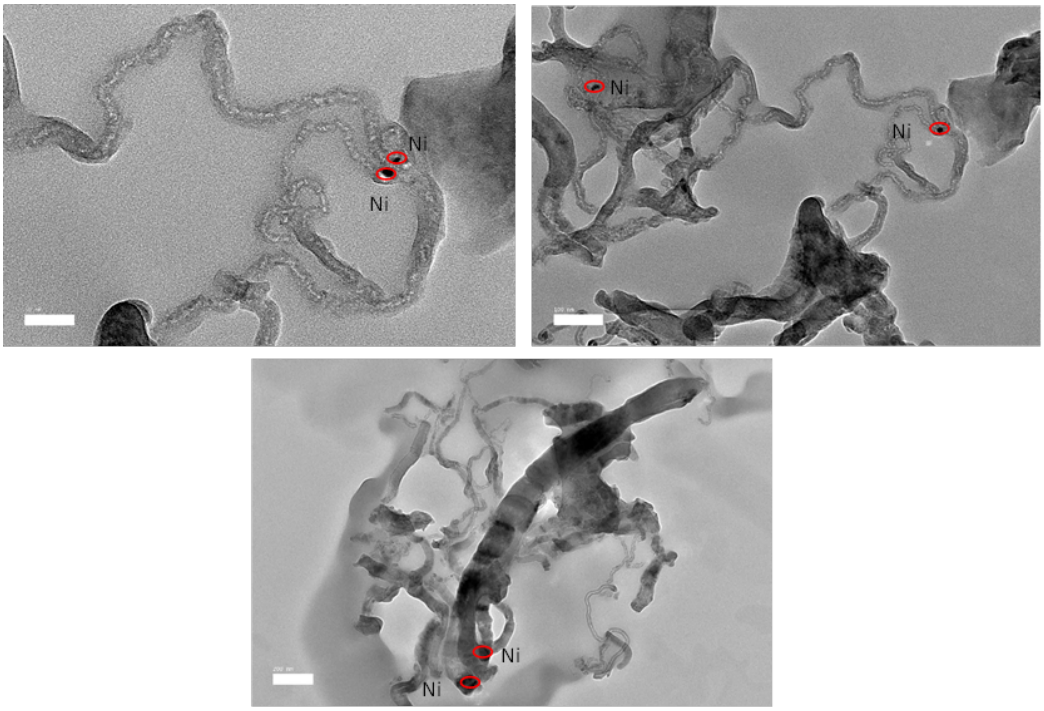

Fig. 4. Microstructure observation of CNTs monolith.

have shown a shift in function groups, including the various modes of vibration between atom groups and structures. The spectrum revealed a change in functional groups, which included the different vibration modes of atomic groups and structures. As shown in Fig. 5(a) and (b), the FTIR spectrum for bare cordierite monolith as well as furfuryl alcohol demonstrated strong peak. However, due to the poor infrared transmittance of CNTs, the FTIR spectra of CNT monoliths revealed a very weak peak, as shown in Fig. 5(c), and appeared to be similar to MWCNTs reported by Haniyeh et al. [47]. The main spectrum presents the absorbance peaks at wavelength 3600 to 3200 cm^{-1} (stretching of O-H functional group), 3000 to 2700 cm^{-1} (stretching of $C-H$ functional group), and wavenumbers 1500-900 cm^{-1} (C-O functional group) as general [48]. The spectrum < 1000 cm^{-1} assigned for metal oxide nanoparticles and usually the peaks appear around 400 and 700 cm^{-1} depending on the type of metal oxide [49].

The peaks at 3720 cm^{-1} became weaker after the CNTs growth onto the monolithic surface, indicating the absence of unbound and free hydroxyl groups [50]. Broad peaks at about 3329 cm^{-1} and 3440 cm^{-1} showed the O-H stretching of hydroxyl groups from carboxyl groups ($O=C-OH$ and $C-OH$), which were related to surface carboxylic, adsorbed water, and intermolecular hydrogen-bonded $OH:OH$ [48]. The presence of a carboxyl group on the surface of CNTs could possibly be due to partial

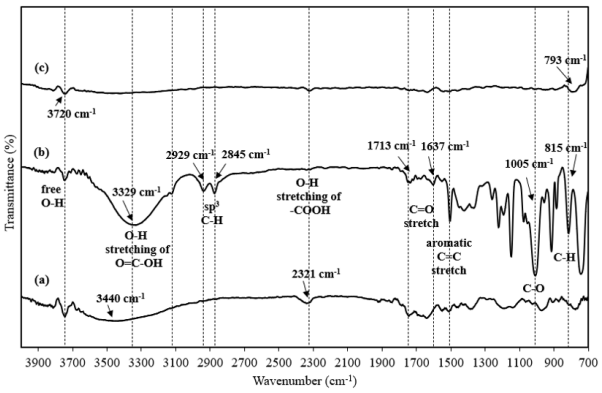

Fig. 5. FTIR profile of (a) bare cordierite monolith, (b) furfuryl alcohol (carbon source) and (c) CNTs monolith.

oxidation during synthesis [51]. The peaks of 2845 cm^{-1} and 2929 cm^{-1} were exhibited only for furfuryl alcohol and described the symmetric and asymmetric vibration of the methylene bonds of the $-CH_2OH$ groups in furfuryl alcohol [52]. Moreover, the O-H stretch from strongly hydrogen-bonded - COOH could be linked to the peak at 2321 cm^{-1} [50]. The peak at 1713 cm^{-1} was assigned for $C=O$ stretching in carbonyl or carboxyl group [53]. While peaks at 1637 cm^{-1} attributed to the aromatic like $C=C$ stretching mode of the CNTs graphitic layers or carbonyl groups [54]. The backbones of CNTs which assigned to

C = C stretching vibration referring to peak 1540 cm^{-1} [55]. The strong peaks at 1005 cm^{-1} and 815 cm^{-1} attributed to the C − O methylol groups and vibration of C − H of furan rings respectively [52]. The peak at 793 cm^{-1} observed at CNTs monolith spectrum assigned as Ni oxide nanoparticles which acts as a catalyst in the synthesizing of CNTs on the monolith [49]. Fig. 5(c) describes that all the peaks are greatly lowered as furfuryl alcohol decomposed into carbon nanotubes (CNTs) on the surface of the cordierite monolith.

The number of immersions is taken into consideration in the EDX spectrum for the CNT monolith as shown in Fig. 6. Fig. 6(a) shows the carbon deposition on the monolithic surface from one-time immersion and Fig. 6(b) shows the carbon deposition from two-time immersions. The two-time immersion contributed to a higher dispersion of metal catalyst onto the surface, thus enhancing the growth of the CNTs. Therefore, Lee et al. [56] found that the repetition of immersion technique for dispersing more Ni catalyst onto the monolith was comparable with the which observed that the thickness of the catalyst has a linear relationship between nanoparticles and diameter of the nanotubes. Therefore, the thickness was strongly affected by the CNTs nanotubes diameter, and the morphology of the nanoparticles formed during the process without influencing the quality of the CNTs.

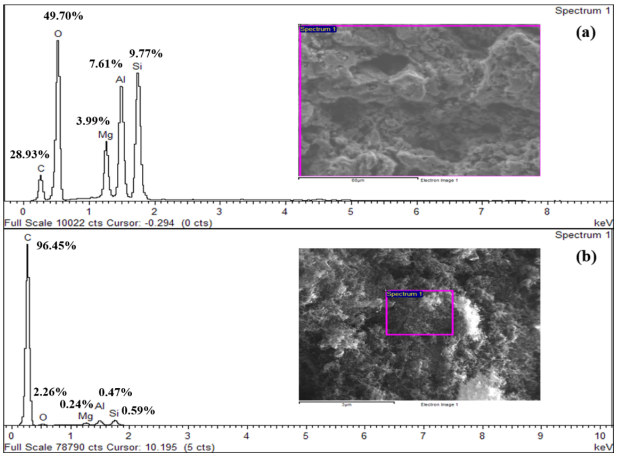

Fig. 6. EDX spectrum of CNTs monolith via (a) one-time immersion and (b) two-time immersion.

3.3. Surface analysis of CNTs monolith

The catalyst performance was significantly impacted by the surface analysis, which is crucial to adsorption. The number of walls, tube diameter, surface functionalization, metal, and amorphous carbon impurities contribute to the different surface area resulted by the CNTs' properties [57]. Using the N_2 adsorption/desorption isotherm, the BET specific surface area, pore size, and pore volume distribution of the bare monolith and CNTs monolith samples were examined. The isotherm of all classified samples, as depicted in Fig. 7(a) and (b), in which two branches are parallel over a wide range of the P/Po due to IUPAC standard classification. The presence of mesoporous structure indicates the isotherm of the bare monolith and CNTs exhibit type IV isotherm accompanied by hysteresis H3. [58] discussed that in the case of mesoporous adsorbents lacking macropores, the type IV isotherm showed that the samples remained almost horizontal throughout the higher relative pressure range. This type of isotherm describes how the adsorption behavior in mesopores is determined by the adsorbent-adsorptive interaction and the interaction between molecules in the condensate. The initial monolayer-multilayer adsorption on the mesoporous walls follows the same route as Type II. The isotherm of synthesized CNTs monolith via immersion-CVD technique observed the relative pressure range at $P/Po > 0.4$ which is similar to Malekbala et al. [32] and Di et al. [59]. Moreover, the isotherm of each type of CNTs monolith has low adsorption compared to Tian et al. [60] which reported the specific surface area (SSA) of CNTs prepared by the hydrothermal method using ammonia, hydrogen peroxide and a metal catalyst with more than 200 m^2/g. The pore size distribution curves of CNTs monolith are illustrated in Fig. 7(b).

As agreed by Kang and Moon, the BET value reveals an SSA value of 15.12 m^2/g [54] who reported that, in comparison to activated carbon, the CNTs had a very small specific area. The CNTs growth onto the monolithic surface increased the surface area about 35% of the clean bare monolith. Numerous impurities including amorphous carbon particles, multilayer polygonal particles, and large graphite platelet were attributed to the low results of MWCNTs surface area. All the BET surface area, pore area, and pore volume were calculated from the pore size distribution curves from the desorption curves of the isotherm via the BJH approach, as shown in Table 1.

3.4. Thermal analysis of CNTs monolith

Fig. 8 displays the results of the thermogravimetric analysis of the CNT monolith. CNT monolith sample degradation occurred in two decreasing phases and one increment phase that contribute to moisture content, organic content, and oxidation of metal catalysts, respectively. According to the results, the moisture content of the CNT monolith was only 0.13 wt.%. While the organic residue and/or solvent capture inside the CNTs monolith samples were eliminated at a temperature higher than 400°C in a nitrogen atmo-

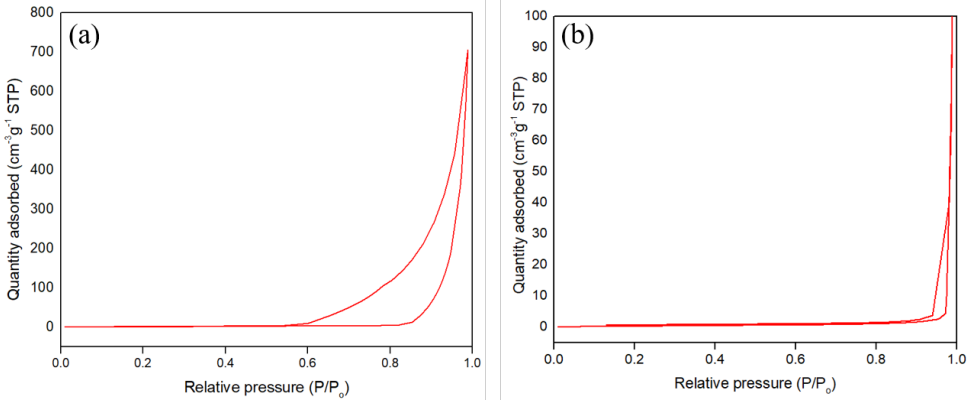

Fig. 7. Nitrogen adsorption-desorption isotherms of (a) bare cordierite monolith and (b) CNTs monolith.

Table 1. Comparison of time performance and performance with different superpixel methods

Types	[a] BET surface area (m^2/g)	[b] Pore volume (cm^3/g)	Pore size (nm)
clean bare monolith	11.1400	1.088706	3909.174
CNTs monolith	15.1178	0.106425	5029.365

[a] calculated by BET equation
[b]BJH desorption pore volume

sphere, only 3wt% mass loss was observed upon heating to 900°C. Findings from previous research by Kang and Moon [61] were found to be similar where a 5% mass loss was seen after the TGA analysis of CNTs balls was removed at 400°C. It was discovered that the initial degradation temperature of CNTs was 400°C, while the greatest weight loss occured at 620°C and degradation was completed at roughly 640°C. This is because of all the carbonaceous material that had been removed and the remaining small amount of metal catalyst that was left behind. After heating the CNTs monolith to 640°C there was an increase of 0.28% mass. This may be attributed to the metal content, which is nickel oxide that remained after the evaporation of carbon material. [62].

3.5. Crystallinity phase determination analysis of CNTs monolit

Fig. 9(a) and (b) depict the X-ray diffraction (XRD) patterns of bare cordierite monolith and the CNTs development onto monolith, respectively. Most of the strong XRD patterns portrayed in Fig. 9(a) were associated with the cordierite phase. (ICDD (International Centre for Diffraction Data) file No. 00-012-0303). The patterns demonstrated that there is only a slight distinction between the CNT phase pattern reflection at $2\theta = 26.46°(002)$ and $44.60°(004)$ according to ICDD file No.00-001-0646 with a hexagonal crystal system [63]. However, there is a notable difference in peak as compare the peak at $2\theta = 25$ to $30°$. The reduction of peak at $2\theta = 26.46°$ after the synthesizing of CNTs growth onto monolith structure was due to the generation of carbon, as seen in Fig. 9(b). During the preparation, the citric acid which is a weak acid functions as a chelating agent for the catalyst in the synthesis process. However, there's no acid treatment onto the cordierite monolithic surface. Therefore, if the material was submerged in an acidic condition, Al, Si, and Mg would not leach. Since both Al and Mg have a basic character, they would leach more readily in a strong acid than Si [64].

4. Conclusions

The CNTs monolith structure by the injection CVD approach could be successfully created and analysis was done for characterization. The technique of immersion combined with the repetition process might facilitate the formation of CNTs on the monolithic surface. Based on all analyses, the characterization has shown that CNTs can be elaborated on the monolith structure. However, the CNTs contain impurities as the synthesis method is without a purifying procedure. As the recommendation, the purification process from amorphous carbon could improve the characteristic of CNTs onto monolith. It is therefore possible to achieve carbon catalyst support with high surface area of CNTs.

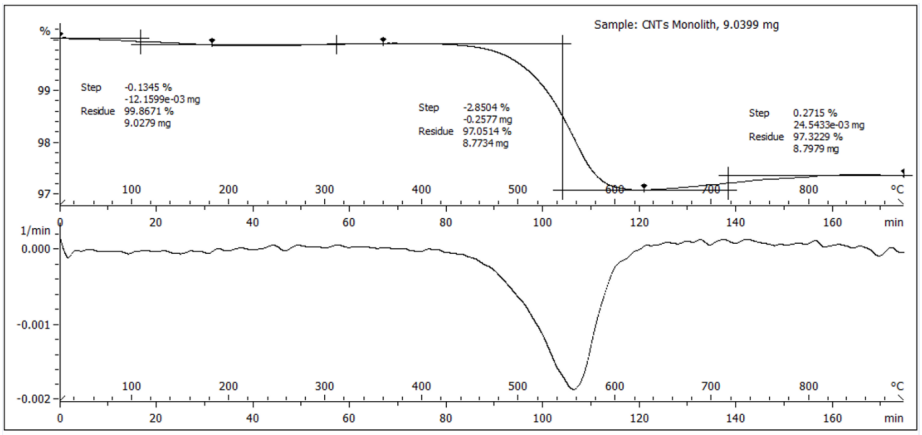

Fig. 8. TGA analysis of CNTs coated onto monolith.

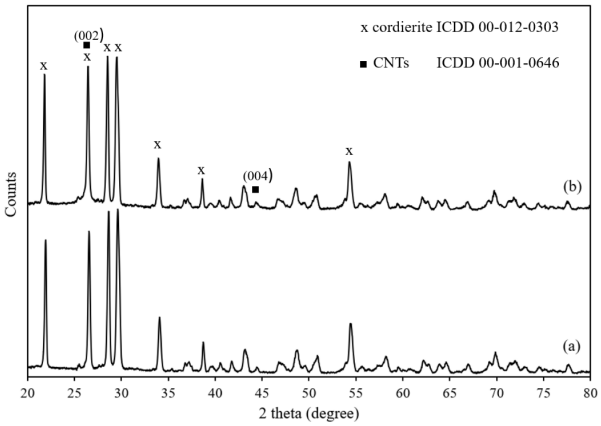

Fig. 9. XRD pattern of (a) bare cordierite monolith and (b) CNTs monolith.

Acknowledgements

The authors gratefully acknowledge the financial assistance provided by Universiti Putra Malaysia for Grant no. GP-IPB/2016/9515202. The authors also acknowledge the Department of Chemical and Environmental Engineering, Faculty of Engineering, Universiti Putra Malaysia for the lab facilities and technical supports. Special thanks to those who contributed to this project directly or indirectly.

References

[1] J. Tang, (2020) *"Carbon nanotube-based flexible electronics"* **Flexible, Wearable, and Stretchable Electronics**: 137–156. DOI: 10.1201/9780429263941-5.

[2] R. Maheswaran and B. P. Shanmugavel, (2022) *"A critical review of the role of carbon nanotubes in the progress of next-generation electronic applications"* **Journal of Electronic Materials** ***51***(6): 2786–2800. DOI: 10.1007/S11664-022-09516-8.

[3] S. Zhu, J. Sheng, Y. Chen, J. Ni, and Y. Li, (2021) *"Carbon nanotubes for flexible batteries: recent progress and future perspective"* **National Science Review** *8*(5): nwaa261. DOI: 10.1093/nsr/nwaa261.

[4] R. Amin, P. R. Kumar, and I. Belharouak. *Carbon Nanotubes–Redefining the World of Electronics*. 2020.

[5] E. Vázquez and M. Prato, (2010) *"Functionalization of carbon nanotubes for applications in materials science and nanomedicine"* **Pure and Applied Chemistry** *82*(4): 853–861. DOI: 10.1351/PAC-CON-09-10-40/html.

[6] B. O. Murjani, P. S. Kadu, M. Bansod, S. S. Vaidya, and M. D. Yadav, (2022) *"Carbon nanotubes in biomedical applications: current status, promises, and challenges"* **Carbon Letters** *32*(5): 1207–1226. DOI: 10 . 1007 / s42823-022-00364-4.

[7] V. Raphey, T. Henna, K. Nivitha, P. Mufeedha, C. Sabu, and K. Pramod, (2019) *"Advanced biomedical applications of carbon nanotube"* **Materials Science and Engineering: C** ***100***: 616–630. DOI: 10.1016/j.msec.2019.03.043.

[8] M.-S. Hong, Y. Park, T. Kim, K. Kim, and J.-G. Kim, (2020) *"Polydopamine/carbon nanotube nanocomposite coating for corrosion resistance"* **Journal of Materiomics** *6*(1): 158–166. DOI: 10.1016/j.jmat.2020.01.004.

[9] A. Kubley, M. Chitranshi, X. Hou, and M. Schulz, (2021) *"Manufacturing and Characterization of Customizable Flexible Carbon Nanotube Fabrics for Smart Wearable Applications"* **Textiles** *1*(3): 534–546. DOI: 10.3390/textiles1030028.

[10] M. Romero-Sáez, A. Dongil, N. Benito, R. Espinoza-González, N. Escalona, and F. Gracia, (2018) *"CO2 methanation over nickel-ZrO2 catalyst supported on carbon nanotubes: A comparison between two impregnation strategies"* **Applied Catalysis B: Environmental *237***: 817–825. DOI: 10.1016/j.apcatb.2018.06.045.

[11] K. S. Ibrahim, (2013) *"Carbon nanotubes? properties and applications: A review"* **Carbon letters *14***(3): 131–144. DOI: 10.5714/CL.2013.14.3.131.

[12] D. R. Minett, J. P. O'Byrne, M. D. Jones, V. P. Ting, T. J. Mays, and D. Mattia, (2013) *"One-step production of monolith-supported long carbon nanotube arrays"* **Carbon *51***: 327–334. DOI: 10.1016/j.carbon.2012.08.060.

[13] M. Mohammad, A. A. Moosa, J. Potgieter, and M. K. Ismael, (2013) *"Carbon nanotubes synthesis via arc discharge with a Yttria catalyst"* **International Scholarly Research Notices *2013***: DOI: 10.1155/2013/785160.

[14] M. C. Paladugu, K. Maneesh, P. K. Nair, and P. Haridoss, (2005) *"Synthesis of carbon nanotubes by arc discharge in open air"* **Journal of nanoscience and nanotechnology *5***(5): 747–752. DOI: 10.1166/jnn.2005.108.

[15] J. Chrzanowska, J. Hoffman, A. Małolepszy, M. Mazurkiewicz, T. A. Kowalewski, Z. Szymanski, and L. Stobinski, (2015) *"Synthesis of carbon nanotubes by the laser ablation method: Effect of laser wavelength"* **physica status solidi (b) *252***(8): 1860–1867. DOI: 10.1002/pssb.201451614.

[16] T. Kuo, C. Chi, and I. Lin, (2001) *"Synthesis of carbon nanotubes by laser ablation of graphites at room temperature"* **Japanese Journal of Applied Physics *40***(12R): 7147. DOI: 10.1143/JJAP.40.7147.

[17] N. De Greef, L. Zhang, A. Magrez, L. Forró, J.-P. Locquet, I. Verpoest, and J. W. Seo, (2015) *"Direct growth of carbon nanotubes on carbon fibers: Effect of the CVD parameters on the degradation of mechanical properties of carbon fibers"* **Diamond and Related Materials *51***: 39–48. DOI: 10.1016/j.diamond.2014.11.002.

[18] W. Zhang, H. Xie, R. Zhang, M. Jian, C. Wang, Q. Zheng, F. Wei, and Y. Zhang, (2015) *"Synthesis of three-dimensional carbon nanotube/graphene hybrid materials by a two-step chemical vapor deposition process"* **Carbon *86***: 358–362. DOI: 10.1016/j.carbon.2015.01.051.

[19] A. Eatemadi, H. Daraee, H. Karimkhanloo, M. Kouhi, N. Zarghami, A. Akbarzadeh, M. Abasi, Y. Hanifehpour, and S. W. Joo, (2014) *"Carbon nanotubes: properties, synthesis, purification, and medical applications"* **Nanoscale research letters *9***: 1–13. DOI: 10.1186/1556-276x-9-393.

[20] J. A. Isaacs, A. Tanwani, M. Healy, and L. Dahlben, (2010) *"Economic assessment of single-walled carbon nanotube processes"* **Journal of Nanoparticle Research *12***: 551–562. DOI: 10.1007/s11051-009-9673-3.

[21] R. Zhang, Y. Zhang, and F. Wei, (2017) *"Horizontally aligned carbon nanotube arrays: growth mechanism, controlled synthesis, characterization, properties and applications"* **Chemical Society Reviews *46***(12): 3661–3715. DOI: 10.1039/C7CS00104E.

[22] I. Levchenko, Z. Han, S. Kumar, S. Yick, J. Fang, and K. Ostrikov. "Large arrays and networks of carbon nanotubes: morphology control by process parameters". In: *Syntheses and Applications of Carbon Nanotubes and Their Composites*. IntechOpen, 2013. DOI: 10.5772/52674.

[23] C.-M. Seah, S.-P. Chai, and A. R. Mohamed, (2011) *"Synthesis of aligned carbon nanotubes"* **Carbon *49***(14): 4613–4635. DOI: 10.1016/j.carbon.2011.06.090.

[24] A. Melezhik, M. Smykov, E. Y. Filatova, A. Shuklinov, R. Stolyarov, I. Larionova, and A. Tkachov, (2013) *"Synthesis of carbon nanotubes from acetone"* **Theoretical Foundations of Chemical Engineering *47***: 435–443. DOI: 10.1134/S0040579513040131.

[25] D. Ping, C. Wang, X. Dong, and Y. Dong, (2016) *"Co-production of hydrogen and carbon nanotubes on nickel foam via methane catalytic decomposition"* **Applied Surface Science *369***: 299–307. DOI: 10.1016/j.apsusc.2016.02.074.

[26] G. Messina, S. Santangelo, M. G. Donato, M. Lanza, C. Milone, A. Pistone, and S. Galvagno, (2008) *"Multi-walled carbon nanotubes production by ethane decomposition over silica-supported iron-catalysts"* **physica status solidi (a) *205***(10): 2422–2427. DOI: 10.1002/pssa.200723647.

[27] M. Zdrojek, J. Sobieski, A. Duzynska, and J. Judek, (2015) *"Synthesis of Carbon Nanotubes from Propane ÃÃ"* **Chem. Vap. Deposition *21***: 1–5. DOI: 10.1002/cvde.201404329.

[28] Z. Jiang, R. Song, W. Bi, J. Lu, and T. Tang, (2007) *"Polypropylene as a carbon source for the synthesis of multi-walled carbon nanotubes via catalytic combustion"* **Carbon *45***(2): 449–458. DOI: 10.1016/j.carbon.2006.08.012.

[29] C. Zhuo, H. Richter, and Y. A. Levendis, (2018) *"Carbon nanotube production from Ethylene in CO2/N2 environments"* **Journal of Energy Resources Technology *140***(8): 085001. DOI: 10.1115/1.4039328.

[30] A. Hussain, Y. Liao, Q. Zhang, E.-X. Ding, P. Laiho, S. Ahmad, N. Wei, Y. Tian, H. Jiang, and E. I. Kauppinen, (2018) *"Floating catalyst CVD synthesis of single walled carbon nanotubes from ethylene for high performance transparent electrodes"* **Nanoscale *10***(20): 9752–9759. DOI: 10.1039/C8NR00716K.

[31] T. Vergunst, F. Kapteijn, and J. Moulijn, (2002) *"Preparation of carbon-coated monolithic supports"* **Carbon *40***(11): 1891–1902. DOI: 10.1016/S0008-6223(02)00034-9.

[32] M. R. Malekbala, S. Soltani, S. Abdul Rashid, L. C. Abdullah, and T. S. Y. Choong, (2019) *"Study the effect of various wash-coated metal oxides over synthesized carbon nanofibers coated monolith substrates"* **Plos one *14***(7): e0219936. DOI: 10.1371/journal.pone.0219936.

[33] M. H. Rümmeli, A. Bachmatiuk, F. Börrnert, F. Schäffel, I. Ibrahim, K. Cendrowski, G. Simha-Martynkova, D. Plachá, E. Borowiak-Palen, G. Cuniberti, et al., (2011) *"Synthesis of carbon nanotubes with and without catalyst particles"* **Nanoscale research letters *6***: 1–9. DOI: 10.1186/1556-276X-6-303.

[34] Y. D. Lim, A. V. Avramchuck, D. Grapov, C. W. Tan, B. K. Tay, S. Aditya, and V. Labunov, (2017) *"Enhanced carbon nanotubes growth using nickel/ferrocene-hybridized catalyst"* **ACS omega 2**(9): 6063–6071. DOI: 10.1021/acsomega.7b00858.

[35] J. Meng, Z. Miao, J. Zhang, Z. Wang, R. Zhang, L. Xu, L. Diao, J. Zhou, and S. Zhuo, (2023) *"One-step synthesis of N-doped carbon nanotubes-encapsulated Ni nanoparticles for efficient electrochemical CO2 reduction to CO"* **Journal of Alloys and Compounds *939***: 168798.

[36] Q. Liu, B. Bian, J. Fan, and J. Yang, (2018) *"Cobalt doped Ni based ordered mesoporous catalysts for CO2 methanation with enhanced catalytic performance"* **international journal of hydrogen energy *43***(10): 4893–4901. DOI: 10.1016/j.ijhydene.2018.01.132.

[37] C.-M. Chen, Y.-M. Dai, J. G. Huang, and J.-M. Jehng, (2006) *"Intermetallic catalyst for carbon nanotubes (CNTs) growth by thermal chemical vapor deposition method"* **Carbon *44***(9): 1808–1820. DOI: 10.1016/j.carbon.2005.12.043.

[38] S. Hosseini, H. Moghaddas, S. M. Soltani, and S. Kheawhom, (2020) *"Technological applications of honeycomb monoliths in environmental processes: a review"* **Process Safety and Environmental Protection *133***: 286–300. DOI: 10.1016/j.psep.2019.11.020.

[39] O. Qistina, A. Salmiaton, T. S. Choong, Y. H. Taufiq-Yap, and S. Izhar, (2020) *"Optimization of carbon nanotube-coated monolith by direct liquid injection chemical vapor deposition based on taguchi method"* **Catalysts *10***(1): 67. DOI: 10.3390/catal10010067.

[40] T. A. Nijhuis, A. E. Beers, T. Vergunst, I. Hoek, F. Kapteijn, and J. A. Moulijn, (2001) *"Preparation of monolithic catalysts"* **Catalysis Reviews *43***(4): 345–380. DOI: 10.1081/CR-120001807.

[41] J. Liu. *"Carbon nanotubes developed on ceramic constituents through chemical vapour deposition"*. (phdthesis). Loughborough University, 2012.

[42] W. Gao, Y. Wan, Y. Dou, and D. Zhao, (2011) *"Synthesis of partially graphitic ordered mesoporous carbons with high surface areas"* **Advanced Energy Materials *1***(1): 115–123. DOI: 10.1002/aenm.201000009.

[43] N. Saifuddin, A. Raziah, and A. Junizah, (2013) *"Carbon nanotubes: a review on structure and their interaction with proteins"* **Journal of Chemistry *2013***: DOI: 10.1155/2013/676815.

[44] C. He, N. Zhao, X. Du, C. Shi, J. Li, and F. He, (2008) *"Characterization of bamboo-shaped CNTs prepared using deposition-precipitation catalyst"* **Materials Science and Engineering: A *479***(1-2): 248–252. DOI: 10.1016/j.msea.2007.06.048.

[45] R. Baker, J. Chludzinski Jr, N. Dudash, and A. Simoens, (1983) *"The formation of filamentous carbon from decomposition of acetylene over vanadium and molybdenum"* **Carbon *21***(5): 463–468. DOI: 10.1016/0008-6223(83)90138-0.

[46] A. Oberlin, M. Endo, and T. Koyama, (1976) *"Filamentous growth of carbon through benzene decomposition"* **Journal of crystal growth *32***(3): 335–349. DOI: 10.1016/0022-0248(76)90115-9.

[47] F. Haniyeh, A. Abdollah, and D. Abolghasem, (2013) *"Controlled growth of well-Aligned carbon nanotubes, electrochemical modification and electrodeposition of multiple shapes of gold nanostructures"* **Materials Sciences and Applications *2013***: DOI: 10.4236/msa.2013.411083.

[48] A. Munajad, C. Subroto, and Suwarno, (2018) *"Fourier transform infrared (FTIR) spectroscopy analysis of transformer paper in mineral oil-paper composite insulation under accelerated thermal aging"* **Energies** ***11***(2): 364. DOI: 10.3390/en11020364.

[49] V. Gupta and T. A. Saleh, (2011) *"Syntheses of carbon nanotube-metal oxides composites; adsorption and photodegradation"* **Carbon Nanotubes-From Research to Applications** ***17***: 295–312. DOI: 10.5772/18009.

[50] M. A. Atieh, O. Y. Bakather, B. Al-Tawbini, A. A. Bukhari, F. A. Abuilaiwi, M. B. Fettouhi, et al., (2010) *"Effect of carboxylic functional group functionalized on carbon nanotubes surface on the removal of lead from water"* **Bioinorganic chemistry and applications** ***2010***: DOI: 10.1155/2010/603978.

[51] F. A. Azri, R. Sukor, R. Hajian, N. A. Yusof, F. A. Bakar, and J. Selamat, (2017) *"Modification strategy of screen-printed carbon electrode with functionalized multi-walled carbon nanotube and chitosan matrix for biosensor development"* **Asian Journal of Chemistry** ***29***(1): 31. DOI: 10.14233/ajchem.2017.20104.

[52] J. Liang, Z. Wu, H. Lei, X. Xi, T. Li, and G. Du, (2017) *"The reaction between furfuryl alcohol and model compound of protein"* **Polymers** ***9***(12): 711. DOI: 10.3390/polym9120711.

[53] D. Vélez, W. Magalhães, and G. Capobianco, (2018) *"Carbon fiber from fast pyrolysis bio-oil"* **Science and Technology of Materials** ***30***: 16–22. DOI: 10.1016/j.stmat.2018.10.001.

[54] A. I. Osman, C. Farrell, A. H. Al-Muhtaseb, J. Harrison, and D. W. Rooney, (2020) *"The production and application of carbon nanomaterials from high alkali silicate herbaceous biomass"* **Scientific reports** ***10***(1): 2563. DOI: 10.1038/s41598-020-59481-7.

[55] R. Yudianti, H. Onggo, Y. Saito, T. Iwata, J.-i. Azuma, et al., (2011) *"Analysis of functional group sited on multi-wall carbon nanotube surface"* **The Open Materials Science Journal** ***5***(1): DOI: 10.2174/1874088X01105010242.

[56] M. W. Lee, M. A. S. M. Haniff, A. S. Teh, D. C. Bien, and S. K. Chen, (2015) *"Effect of Co and Ni nanoparticles formation on carbon nanotubes growth via PECVD"* **Journal of Experimental Nanoscience** ***10***(16): 1232–1241. DOI: 10.1080/17458080.2014.994679.

[57] M. E. Birch, T. A. Ruda-Eberenz, M. Chai, R. Andrews, and R. L. Hatfield, (2013) *"Properties that influence the specific surface areas of carbon nanotubes and nanofibers"* **Annals of occupational hygiene** ***57***(9): 1148–1166. DOI: 10.1093/annhyg/met042.

[58] M. Thommes, K. Kaneko, A. V. Neimark, J. P. Olivier, F. Rodriguez-Reinoso, J. Rouquerol, and K. S. Sing, (2015) *"Physisorption of gases, with special reference to the evaluation of surface area and pore size distribution (IUPAC Technical Report)"* **Pure and applied chemistry** ***87***(9-10): 1051–1069. DOI: 10.1515/pac-2014-1117.

[59] L. Di, H. Yang, T. Xian, and X. Chen, (2018) *"Construction of Z-scheme g-C3N4/CNT/Bi2Fe4O9 composites with improved simulated-sunlight photocatalytic activity for the dye degradation"* **Micromachines** ***9***(12): 613. DOI: 10.3390/mi9120613.

[60] Z. Tian, C. Liu, Q. Li, J. Hou, Y. Li, and S. Ai, (2015) *"Nitrogen-and oxygen-functionalized carbon nanotubes supported Pt-based catalyst for the selective hydrogenation of cinnamaldehyde"* **Applied Catalysis A: General** ***506***: 134–142. DOI: 10.1016/j.apcata.2015.08.023.

[61] D.-Y. Kang and J. H. Moon, (2014) *"Carbon nanotube balls and their application in supercapacitors"* **ACS applied materials & interfaces** ***6***(1): 706–711. DOI: 10.1021/am404960r.

[62] H. A. Asmaly, B. Abussaud, T. A. Saleh, V. K. Gupta, M. A. Atieh, et al., (2015) *"Ferric oxide nanoparticles decorated carbon nanotubes and carbon nanofibers: from synthesis to enhanced removal of phenol"* **Journal of Saudi Chemical Society** ***19***(5): 511–520. DOI: 10.1016/j.jscs.2015.06.002.

[63] F. M. Anjalin, (2014) *"Synthesis and characterization of MWCNTs/PVDF nanocomposite and its electrical studies"* **Der Pharma Chemica** ***6***(1): 354–359.

[64] E. Soghrati, M. Kazemeini, A. Rashidi, and K. J. Jozani, (2014) *"Development of a structured monolithic support with a CNT washcoat for the naphtha HDS process"* **Journal of the Taiwan Institute of Chemical Engineers** ***45***(3): 887–895. DOI: 10.1016/j.jtice.2013.08.009.